5.1 Introduction

This chapter includes tensile test results for five cases, as well as, the experimental and numerical results for fatigue test for the base material, optimum case (single pass), and two passes are discussed in this chapter. In addition, X-ray and Vickers hardness results for the base material, single pass (optimum case) and double pass.

5.2 Tensile Test

The tensile tests were conducted to obtain the values of ultimate strength, proof strength and elongation for both base and welding material for five cases. Case one for base material, three cases depended on the orientation of welding line with applied load (45^o, 60^o and 90^o) and last case for double passes for the optimum parameters.

$$\textbf{Efficiency} = \frac{\sigma_{ut}\ \textbf{for welding}}{\sigma_{ut}\ \textbf{for BM (280 MPa)}} * \mathbf{100\%} \quad \ldots\ldots\ldots\ldots\ldots (\mathbf{5.1})$$

5.2.1 Case One: Tensile Test Results For Base Material

The tensile results for base material are explained in table (**5.1**).

Table (**5.1**) Tensile results for base material.

Material	Ultimate strength (MPa)	Proof strength 0.2% (MPa)	Elongation (%)
Base material	280	255	12
Standard [28]	289	241	15.8

Figure (**5.1**): Orientation fracture for the base material.

5.2.2 Case Two: Tensile Test for OWL 90^{o} With The Applied Load

Table (5.2) the tensile test results and efficiency for OWL 90^{o}.

No	parameter		Ultimate strength (MPa)	Proof strength (MPa)	Elongation (mm)	Weld efficiency %
	R.S (rpm)	W.S (mm/min)				
1	630	20	222.5	148.037	5.3	79.46
		32	218	146.219	5.1	77.857
		45	216.1	154.344	4.2	77.18
2	1000	20	239	142.148	5.6	85.35
		32	234.5	153.2044	5.44	83.75
		45	230	154.204	4.9	82.14
3	1600	20	242	167.34	5.8	86.429
		32	236	142.249	5.5	84.28
		45	231.5	153.797	5.2	82.67

Table (**5.2**) shows reduction in ultimate tensile test for welding when compared with the base material for all rotation and welding speeds. The reduction in tensile strength for welding is due to the different in micro-structure between the weld zones and occurs precipitations and dissolutions in weld, while the base material contain same micro-structure [74].

Figure (**5.2**) shows that increasing rotation speed lead to increase the ultimate tensile strength for all welding speed. This increasing is due to

increase the amount of heat transfer during the weld operation and this heat work on increase refines in micro-structure in welding. Generally, the mechanical properties of the aluminum alloy (6061) are dependent on size and distribution of precipitations compounds and density of compounds (needle-shaped) within the micro-structure of the alloy which works to increase its mechanical properties [37], therefore the decrease in ultimate strength for weldment that welded by 630 rpm and 45 mm/min may be due to a non-homogeneous distribution of precipitations compounds in this weldment.

Figure (**5.3**) shows the relation between the tensile strength and the welding speed, the ultimate strength is reduced with increasing welding speeds for all rotational speeds. This reduction in ultimate tensile strength when increasing welding speeds is due to reduce material flow around the welding tool and the produce non-homogenous metal distribution.

Figure (**5.4**) shows that relation between the elongation and welding speed for all rotation and welding speeds, the weldment has elongation lower than the base material. Elongation is reducing with increase welding speed. This reduction in elongation is due to different microstructure between the weld zones [37]. For all specimens in this case the weld line was perpendicular to the applied load, and the fracture occurs in the advance side. In the sample that welded by 630 rpm rotation speed and the welding speed, 45 mm/min the fracture occurs in regions between TMEZ and SZ as shown in figure (**5.5**). The TMEZ composed of coarse-bent recovered grains while the stir zone composed of fine recrystallized grain and this conform with T. A. Jawed [23] and H.J. Liu [76]. While the others samples the fraction location occurs in the HAZ as shown in figure (**5.5**) due to the significant coarsening of the precipitated and this conforms with Mishra and Ma [18], and Babu [77] as well as, Ren et al. [78]. The fracture orientation is perpendicular to the applied load as shown in figure (**5.5**).

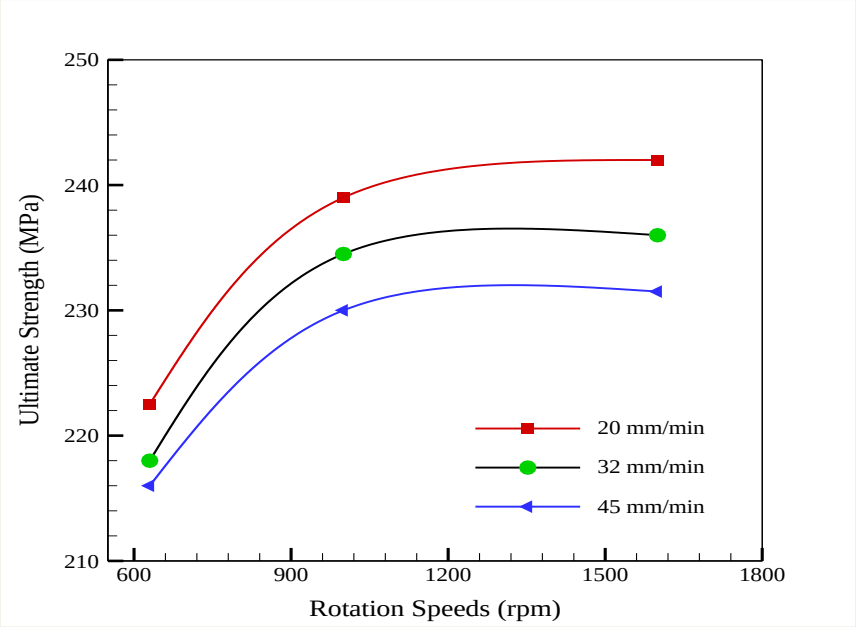

Figure (**5.2**): Ultimate strength-Rotation speed for (90^{o}).

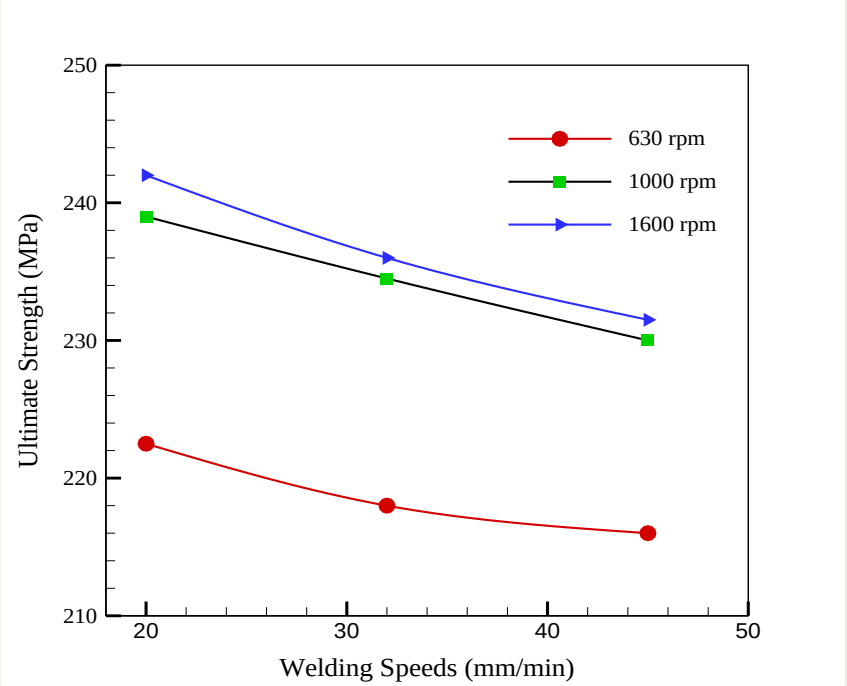

Figure (**5.3**): Ultimate strength-Welding speeds for (90^{o}).

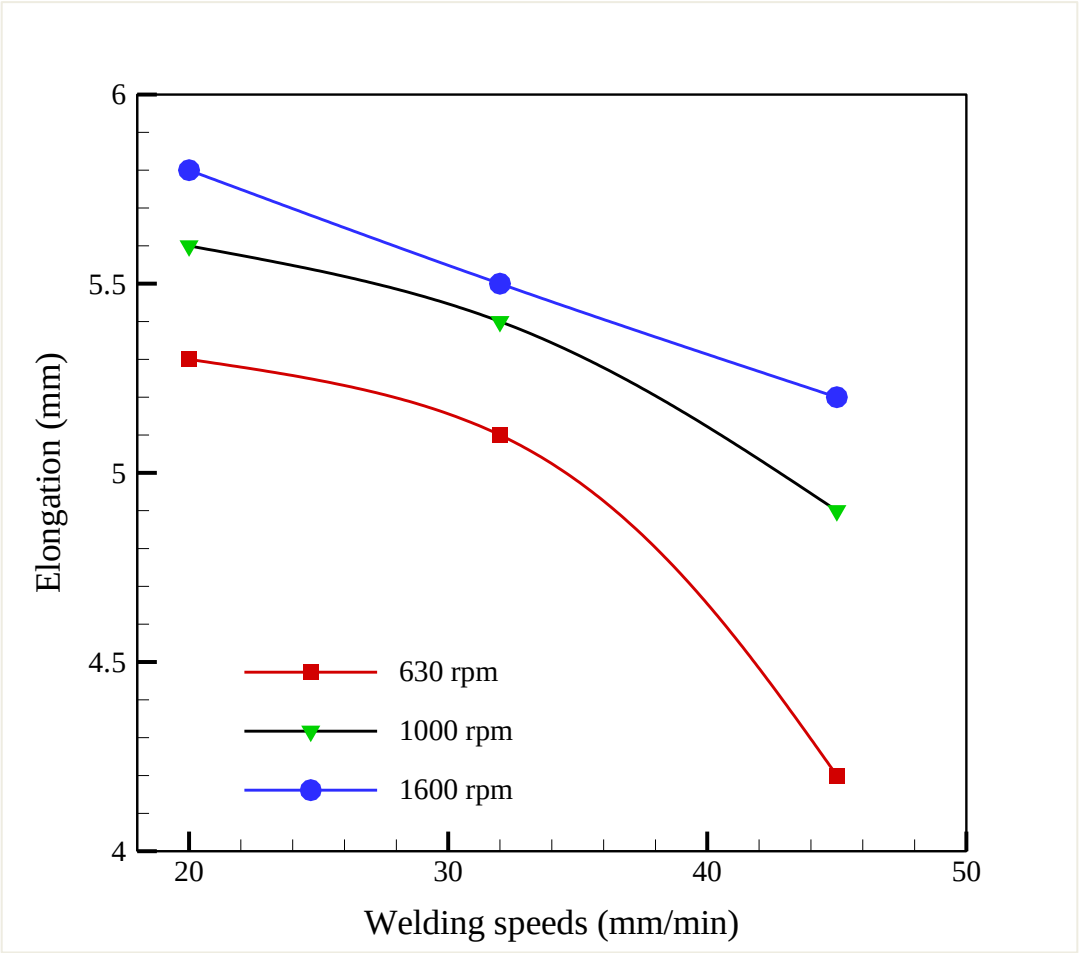

Figure (**5.4**): Elongation- welding speed for (90^{o}).

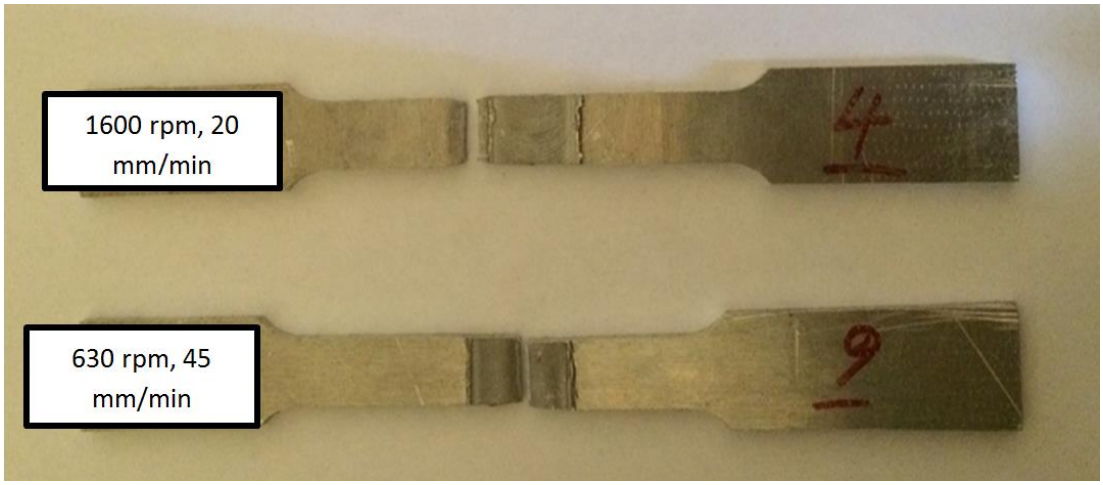

Figure (**5.5**): Orientation fracture for (90^{o}).

5.2.3 Case Three: Tensile Test Results For OWL 60^{o} With Applied Load

Table (**5.3**) the tensile test results and efficiency for OWL 60^{o}.

No	parameter		Ultimate strength (MPa)	Elongation (mm)	Proof strength (MPa)	Weld efficiency (%)
	R.S (rpm)	W.S (mm/min)				
1	630	20	220	6.7	107.16	78.57
		32	215	6.5	124.82	76.6
		45	204	4.4	130.857	73.57
2	1000	20	225.5	6.5	133.767	80.536
		32	214.5	4.52	114.622	76.6
		45	206	3.7	124.82	76.53
3	1600	20	229	7.3	158.04	81.78
		32	225	6.7	119.06	80.35
		45	214.3	4.6	122.4	75

The results showed that reduction in ultimate tensile test for weldment when compared with the base material for all rotation and welding speeds for weldment with OWL 60^{o}. The higher ultimate tensile strength for weldment at this case was 229 MPa with weld efficiency 81.78 % at 1600 rpm and welding speed 20 mm/min. The lowering tensile strength was 204 MPa with 73.57 % at 630 rpm and welding speed 45 mm/min. In this case the ultimate strength reduced with increasing the feed rate (welding speed) and decrease rotation speeds as shown in figure (**5.6**) and (**5.7**). The elongation decreasing with the increasing welding speeds as shown in figure (**5.8**). In this case, most fracture location occurs in advance side in region between SZ and TMAZ, orientation of fracture was ~ 60^{o} with the applied load as shown in figure (**5.9**). Welding efficiency in this case is lower than case one because of increasing in shear stress on welding line.

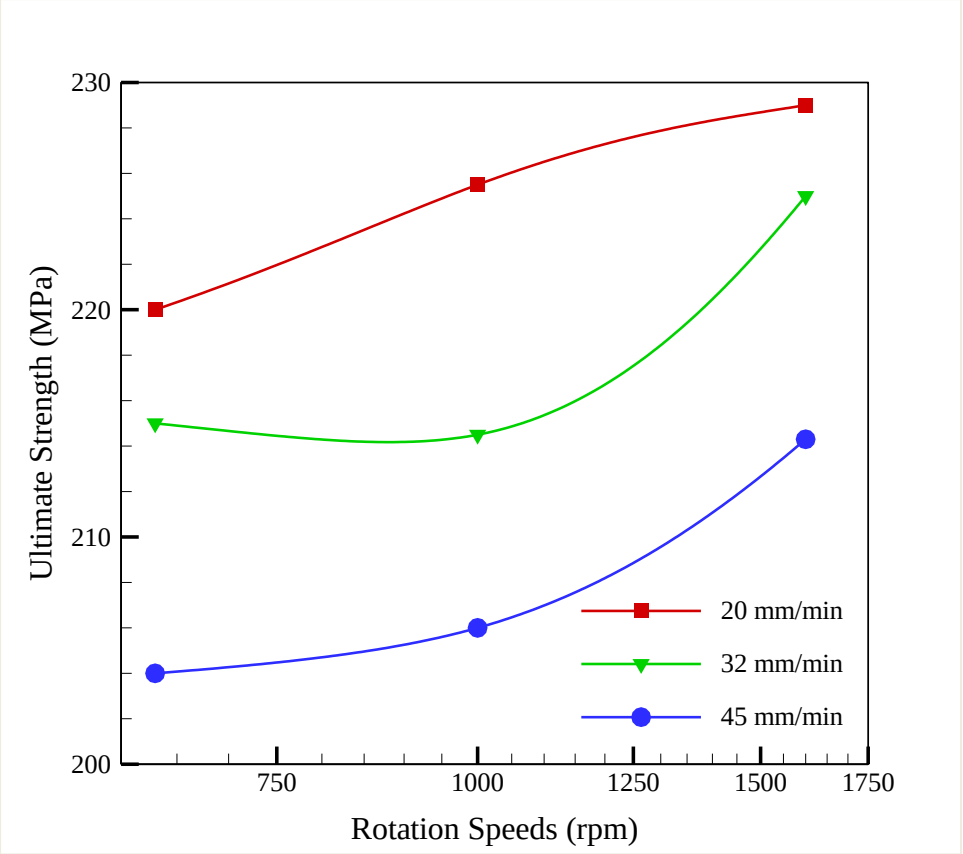

Figure (**5.6**): Ultimate strength- rotation speeds for 60°.

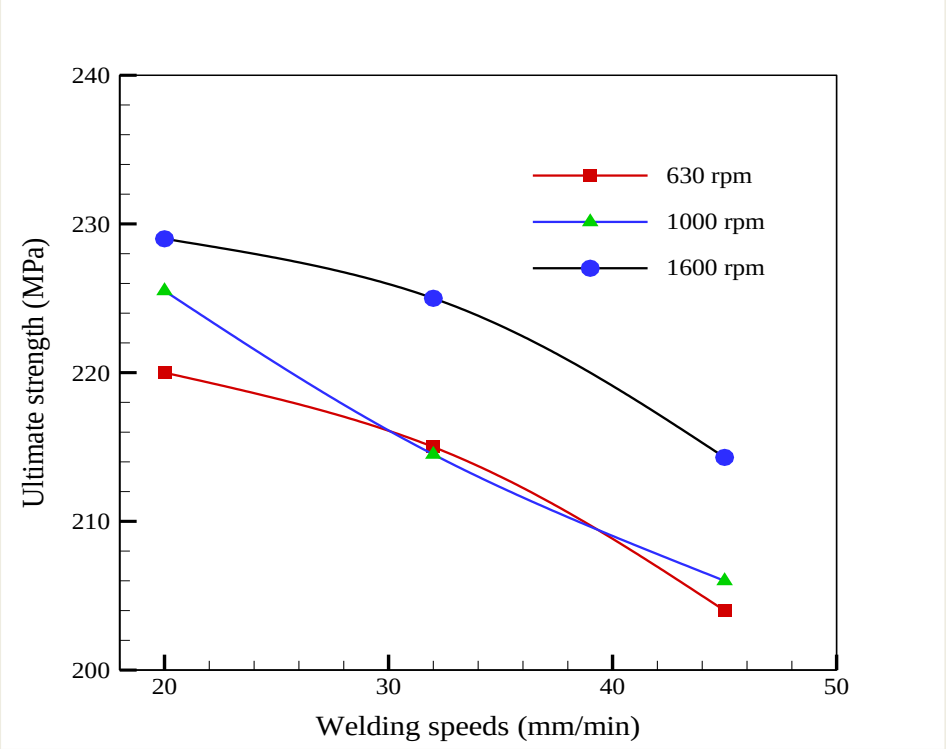

Figure (**5.7**): Ultimate strength – welding speed for 60°.

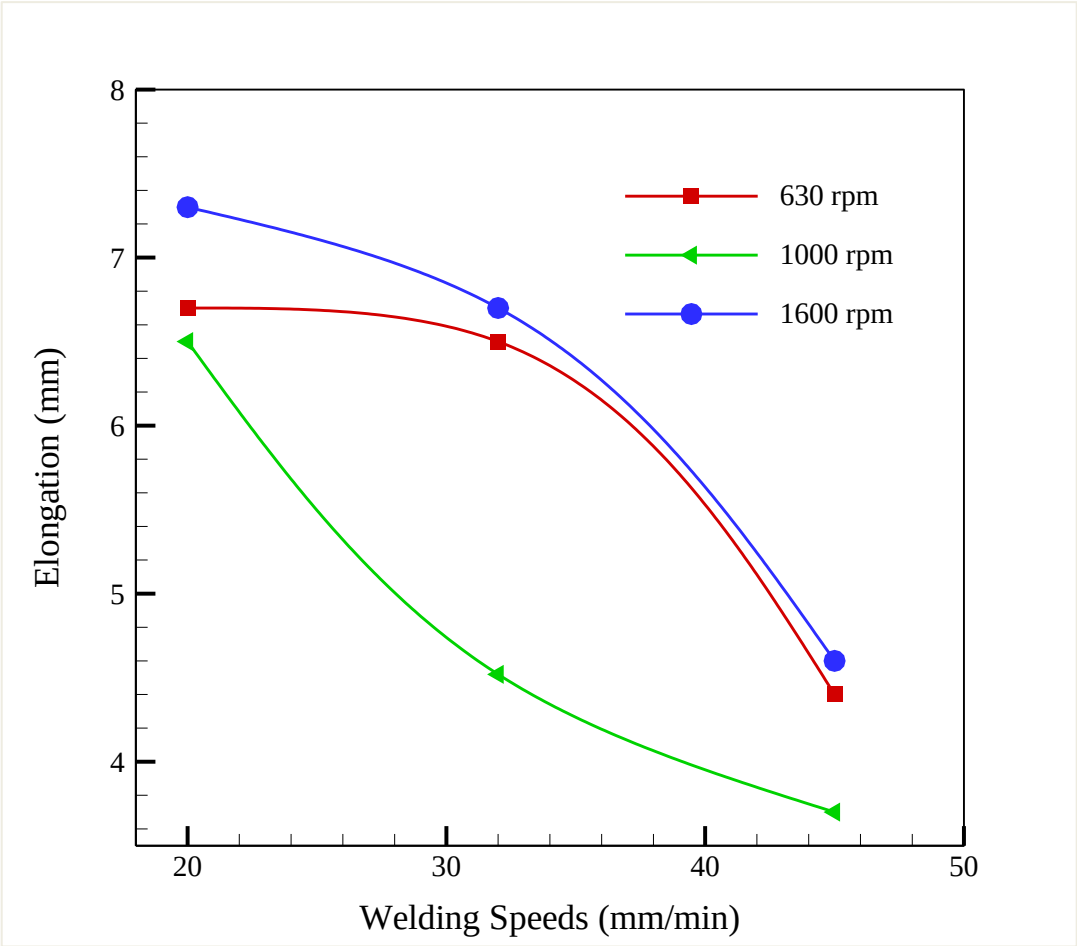

Figure (**5.8**): Elongation- welding speed for 60°.

Figure **(5.9):** Orientation fracture for case three (60°).

5.2.4 Case Four: The OWL 45^{o} With Applied Load

Table (**5.4**) Tensile results for weldment with OWL 45^{o}.

No	parameter		Ultimate strength (MPa)	Proof strength (MPa)	Elongation (mm)	Weld efficiency (%)
	R.S (rpm)	W.S (mm/min)				
1	630	20	212	115.2	6.8	75.71
		32	201	123.917	4.6	71.78
		45	191	126.2005	3.66	68.2
2	1000	20	210	54.304	4.49	75
		32	203.5	145.98	4.17	72.67
		45	188	117.92	3.328	67.14
3	1600	20	218	127.008	8	77.85
		32	210.55	138.3	7.8	75.19
		45	204	100.905	7.67	72.85

Table (**5.2**) shows reduction in ultimate tensile test for welding when compared with the base material for all rotation and welding speeds. The maximum weld efficiency was 77.85 % at 1600 rpm and 20 mm/min while the minimum weld efficiency was 67.14 % at 1000 rpm and 45 mm/min. In this case, the increase rotation speed and decreasing welding speed lead to increase the ultimate strength of the material as shown in figures (**5.10**) and (**5.11**). The elongation reduced with increasing feed rate (welding speed) as shown in figure (**5.12**). The fracture location occurs in advance side in region between SZ and TMAZ for most welding and rotation speeds, the orientation of fracture was ~ 45^{o} with the applied load as shown in figure (**5.13**).

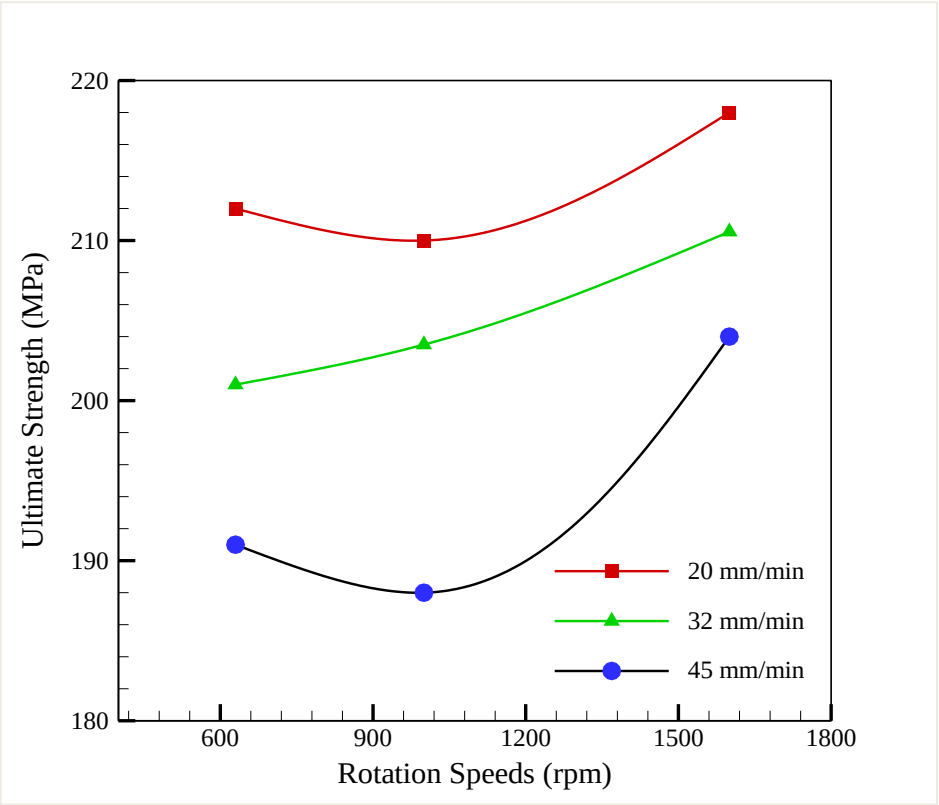

Figure (**5.10**): Ultimate strength-rotation speed for 45°.

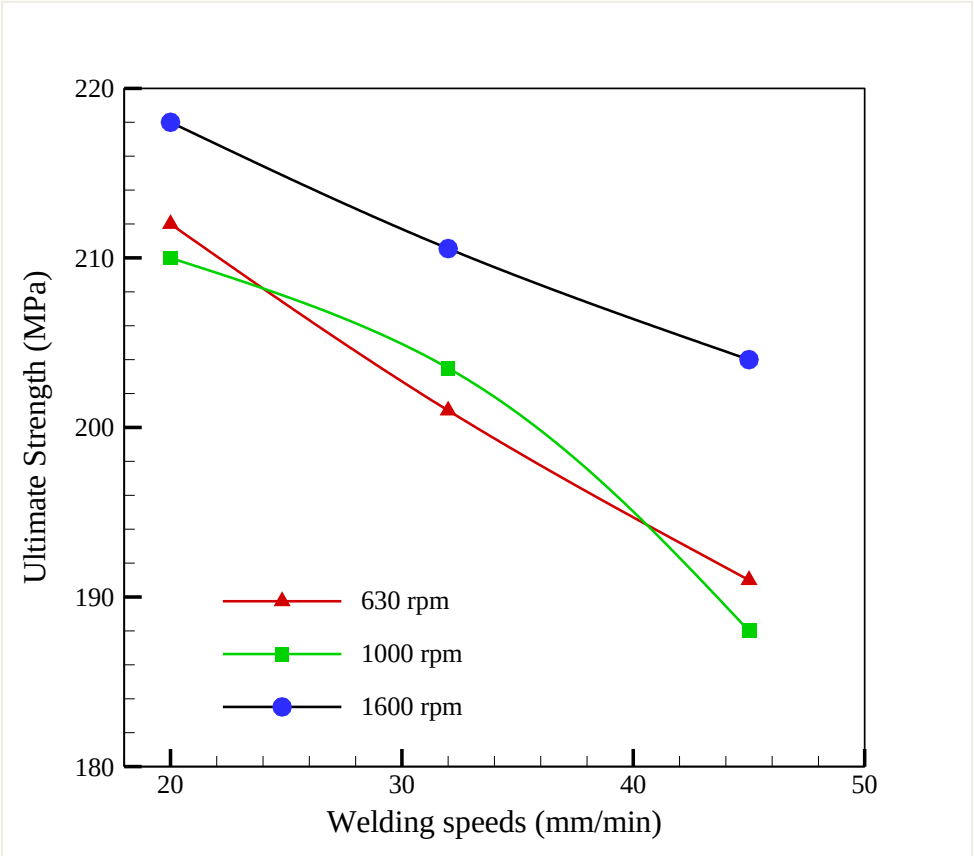

Figure (**5.11**): Ultimate strength-welding speed for 45°.

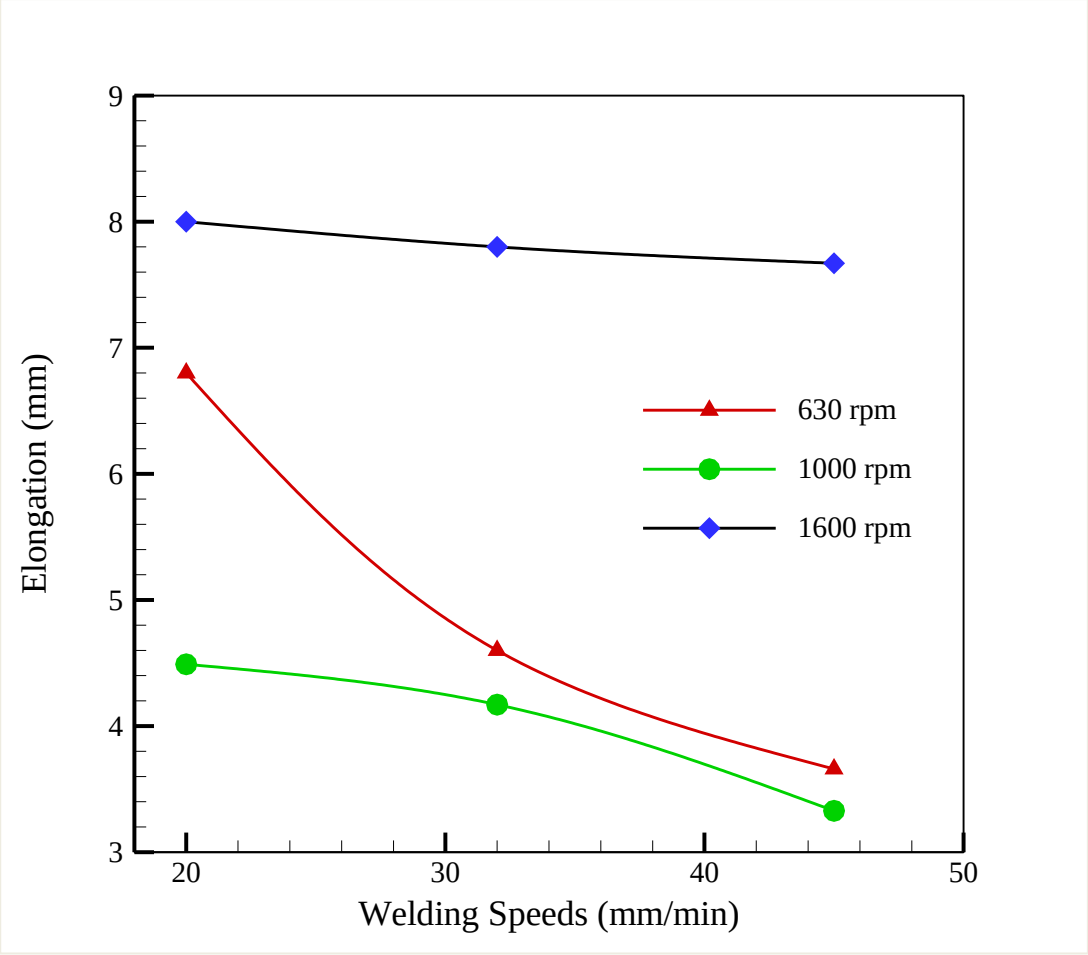

Figure (**5.12**): Elongation- welding speed for OWL 45°.

Figure (**5.13**): Orientation fracture for OWL 45°.

5.2.5 Comparison Between Different Orientation Welding Lines

The Change in orientation welding line (OWL) leads to reduce the weld efficiency and change the position and orientation of fracture in tensile test. The best OWL was at 90^{o} with the applied load while OWL 60^{o} was best from OWL 45^{o} as shown in table (**5.5**). At OWL 45^{o}, 1000 rpm, and 45 mm/min higher reduction in ultimate strength occurs, while the lower reduction in ultimate strength occurs at OWL 60^{o}, 630 rpm, and 20 mm/min. The effect of different OWL (60^{o} and 45^{o}) on ultimate strength, proof strength, and elongation are lower.

Table (**5.5**) reduction in ultimate strength at OWL 60^{o} and 45^{o}

R.S	W.S	Reduction in ultimate strength at OWL 60^{o} (%)	Reduction in ultimate strength at OWL 45^{o} (%)
630	20	1.12	4.72
	32	1.3	7.7
	45	5.6	11.6
1000	20	5.6	12.13
	32	8.6	13.2
	45	10.43	18.26
1600	20	5.3	9.9
	32	2.3	8.4
	45	7.43	11.88

5.3 Minitab Results

5.3.1 Single to Noise

From Minitab results, the optimum case (single pass) to get on higher ultimate strength was at 1600 rpm rotation speed and 20 mm/min welding speed, while the orientation of welding line 90^{o}, and to get on higher proof strength was at 1600 rpm and 32 mm/min while OWL 90^{o}, while the optimum parameter to get on higher elongation was at 1600 rom, 20 mm/min, and OWL 60^{o}, its shown in figure (**5.14**). S/N ratio results for tensile strength, proof strength, and elongation are explained in table (**5.6**). Lower range of welding speed is appropriate for achieving superior mechanical properties and results higher ductility and elongation [39, 79]. All details explained in appendix A.

Table (**5.6**) S/N ratio and mean results of tensile strength, proof strength and elongation.

Worksheet 2 ***

↓	C1	C2	C3	C4	C5	C6	C7	C8	C9	C10	C11	C12
	R.S	W.S	OWL	ult. str.	proof. str.	elongation	SNRA1	MEAN1	SNRA2	MEAN2	SNRA3	MEAN3
1	630	20	45	212.00	115.200	6.800	46.5267	212.00	41.2290	115.200	16.6502	6.800
2	630	20	60	220.00	107.160	6.700	46.8485	220.00	40.6007	107.160	16.5215	6.700
3	630	20	90	222.50	148.037	5.300	46.9466	222.50	43.4074	148.037	14.4855	5.300
4	630	32	45	201.00	123.917	4.600	46.0639	201.00	41.8626	123.917	13.2552	4.600
5	630	32	60	215.00	124.820	6.500	46.6488	215.00	41.9257	124.820	16.2583	6.500
6	630	32	90	218.00	146.219	5.100	46.7691	218.00	43.3001	146.219	14.1514	5.100
7	630	45	45	191.00	126.201	3.660	45.6207	191.00	42.0213	126.201	11.2696	3.660
8	630	45	60	204.00	130.857	4.400	46.1926	204.00	42.3359	130.857	12.8691	4.400
9	630	45	90	216.10	154.330	4.200	46.6931	216.10	43.7690	154.330	12.4650	4.200
10	1000	20	45	210.00	54.000	4.490	46.4444	210.00	34.6479	54.000	13.0449	4.490
11	1000	20	60	225.50	133.767	6.500	47.0629	225.50	42.5270	133.767	16.2583	6.500
12	1000	20	90	239.00	142.148	5.600	47.5680	239.00	43.0548	142.148	14.9638	5.600
13	1000	32	45	203.50	145.980	4.170	46.1713	203.50	43.2859	145.980	12.4027	4.170
14	1000	32	60	214.30	114.622	4.520	46.6204	214.30	41.1854	114.622	13.1028	4.520
15	1000	32	90	234.50	153.204	5.440	47.4029	234.50	43.7054	153.204	14.7120	5.440
16	1000	45	45	188.00	117.920	3.328	45.4832	188.00	41.4317	117.920	10.4437	3.328
17	1000	45	60	206.00	124.820	3.700	46.2773	206.00	41.9257	124.820	11.3640	3.700
18	1000	45	90	230.00	154.204	4.900	47.2346	230.00	43.7619	154.204	13.8039	4.900
19	1600	20	45	218.00	127.008	8.000	46.7691	218.00	42.0766	127.008	18.0618	8.000
20	1600	20	60	229.00	158.040	7.300	47.1967	229.00	43.9753	158.040	17.2665	7.300
21	1600	20	90	242.00	167.340	5.800	47.6763	242.00	44.4720	167.340	15.2686	5.800
22	1600	32	45	210.55	138.700	7.800	46.4671	210.55	42.8415	138.700	17.8419	7.800
23	1600	32	60	225.00	119.060	6.700	47.0437	225.00	41.5153	119.060	16.5215	6.700
24	1600	32	90	236.00	142.250	5.500	47.4582	236.00	43.0610	142.250	14.8073	5.500
25	1600	45	45	204.00	100.905	7.670	46.1926	204.00	40.0783	100.905	17.6959	7.670
26	1600	45	60	214.30	122.400	4.600	46.6204	214.30	41.7556	122.400	13.2552	4.600
27	1600	45	90	231.50	153.700	5.200	47.2910	231.50	43.7335	153.700	14.3201	5.200

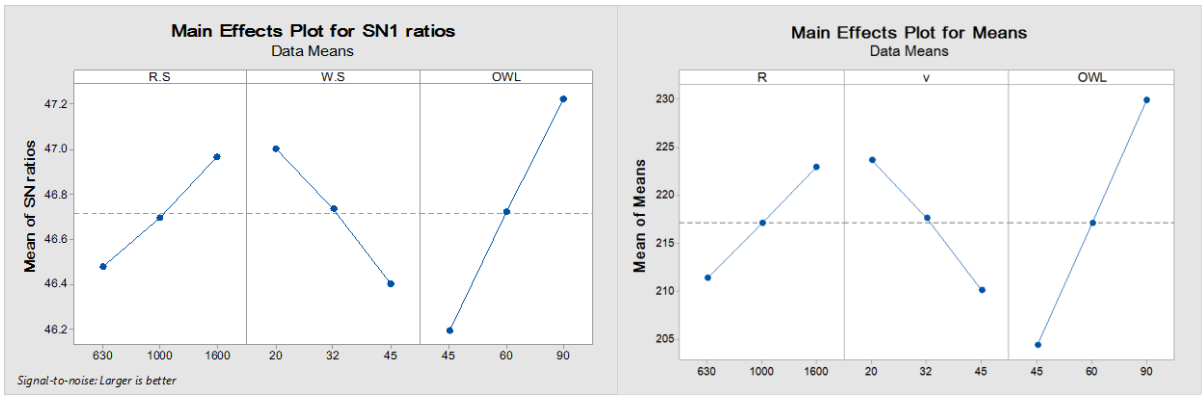

(A)

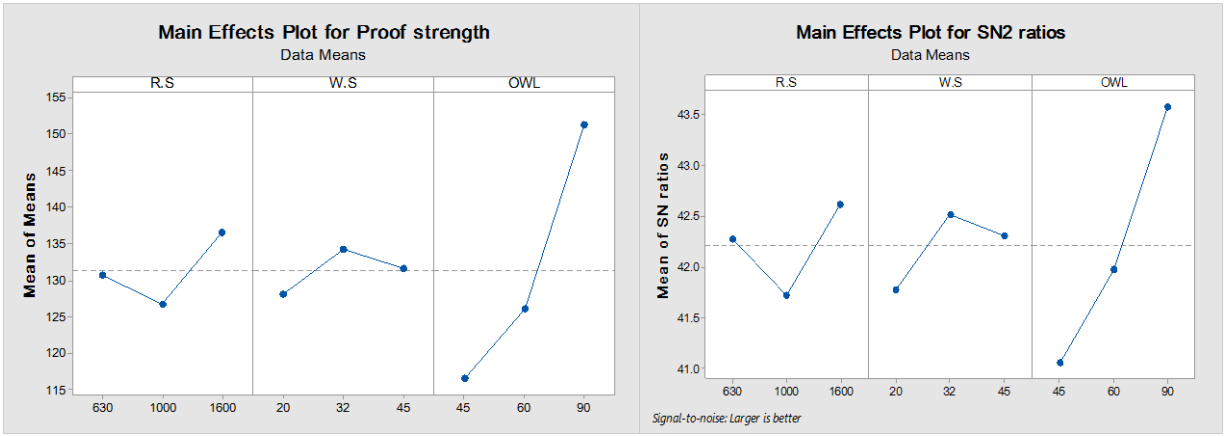

(B)

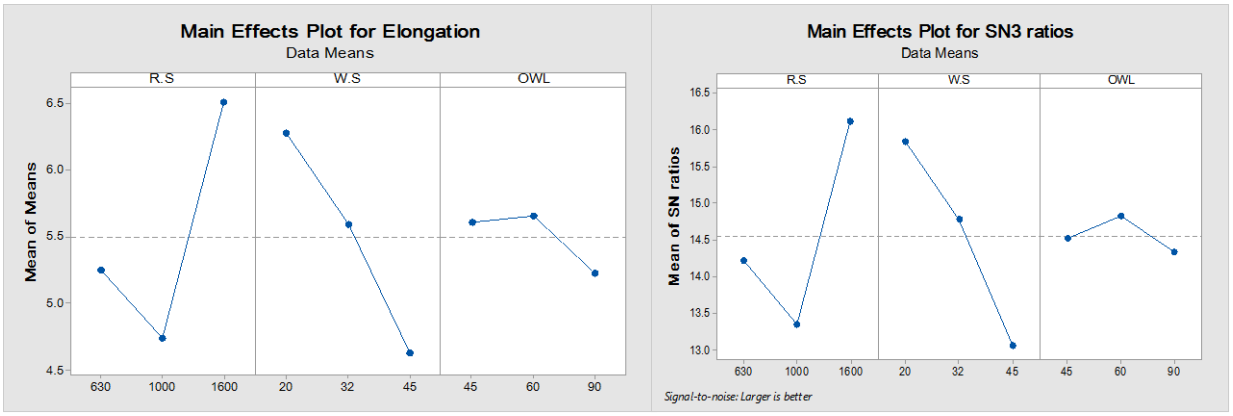

(C)

Figure (**5.14**): Main effect plot for mean tensile strength and S/N ratio for (A) ultimate strength, (B) proof strength, and (C) elongation.

5.3.2 ANOVA Analysis

The percentage contribution for welding speed, OWL, and rotation speed were presented in figure (**5.15**). The OWL has higher effective on ultimate strength and proof strength while has lower effect on elongation.

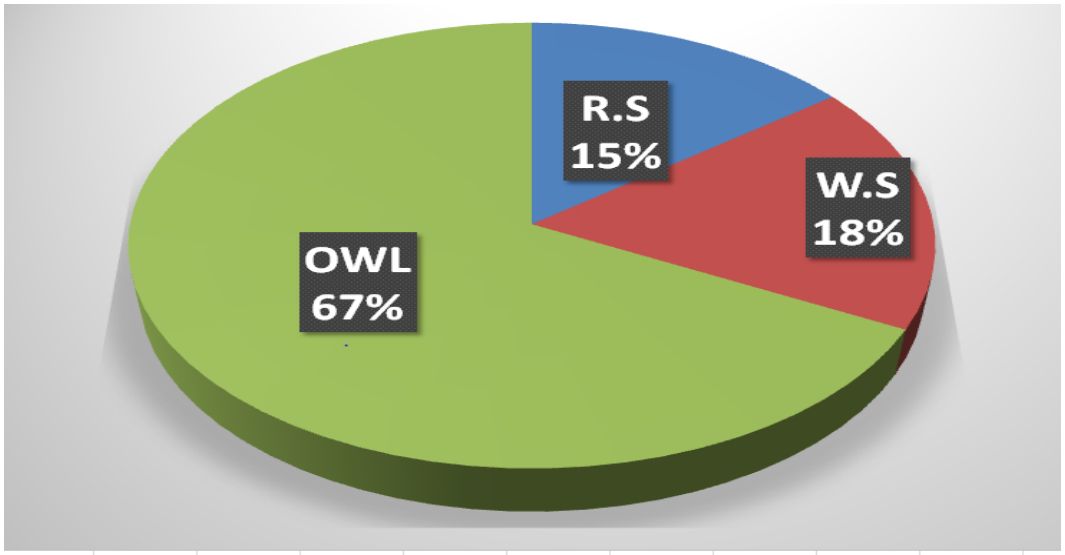

(A)

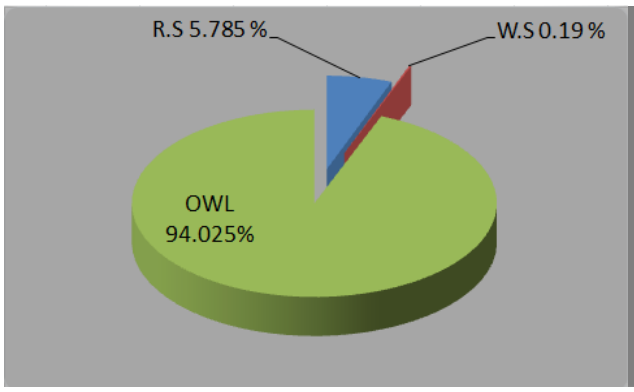

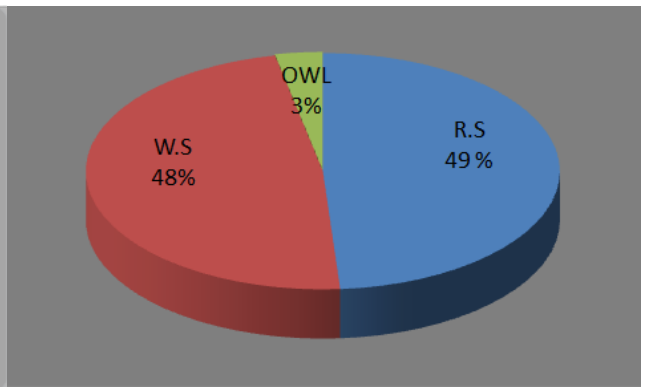

(B) (C)

Figure (**5.15**): effect of welding parameters on (A) ultimate strength, (B) Proof strength, and (C) elongation.

5.4 Case Five: Tensile Test Results For Double Passes:

The double passes used and optimum parameters that give higher ultimate strength only. From table (**5.7**) the ultimate tensile strength for optimum case (single pass) was 242 MPa and elongation was 5.8 mm, but when using double pass (FSP) the ultimate tensile strength increase to 251 MPa to give weld efficiency 89.64% and elongation increased to 9.8 mm. The FSP (double pass) lead to enhance mechanical properties and modification of microstructure [50].

Table (**5.7**): Comparison between single pass and double pass.

Material	Ultimate strength (MPa)	Proof Strength (MPa)	Elongation (mm)	Weld Efficiency (%)
Single Pass	242	168	5.8	86.429
Double Pass	251	178.5	9.8	89.64

5.5 Hardness Test Results

The Vickers Hardness tests were performed for three samples: base material and the single pass (optimum case) for FSW as well as double passes. The operation of welding led to reduce the micro-hardness values when compared with the base material. Figure (**5.16**) explained the results of hardness test for the base material, single pass, and double passes. The hardness for base material was 99.98 HV0.5; it's presented in table (**5.8**). While the minimum hardness for FSW was 50 HV0.5 in HAZ, and the hardness for SZ was 50.6 HV0.5 and this conforms to T. Khaled [13].

This difference in weld zone hardness due to the amount of heat generated which caused softening of HAZ, TMAZ, and NZ due to dissolution and coarsening of the strengthening precipitates during the welding operation

[22]. After the double pass with rotational speed (1600 rpm) and welding speed 20 mm/min. The minimum hardness was 54.5 HV0.5 in HAZ with reduction of about 46.5% from the base material and in SZ was 79.9 HV0.5 with the reduction of about 20% from the base material. The hardness improved in double pass in SZ this return to the effect of the recrystallization and the more fineness of the grains. As well as the micro-hardness is improved in most zones this is due to the double pass worked on reduction tensile residual stresses and homogeneous it on both sides [36].

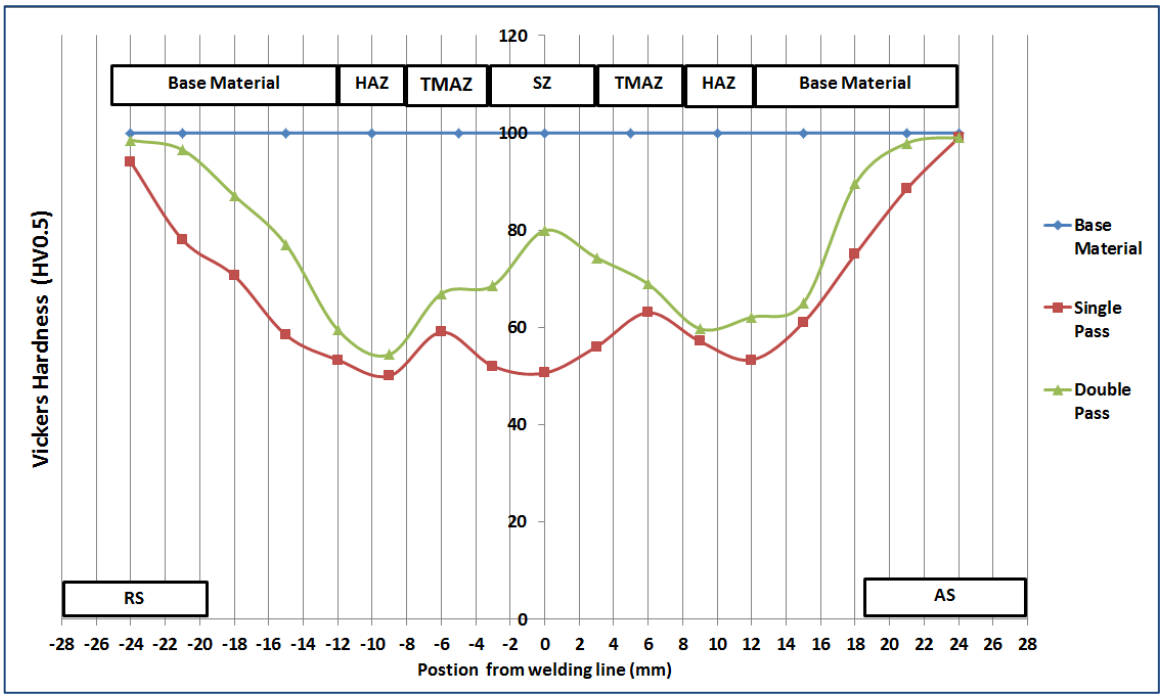

Figure (**5.16**): The Vickers hardness for three cases.

5.6 X-Ray Diffraction Results

The stresses will form in the weld during welding operation since the expansion of materials happens through the heating of the welded plates, followed by the contraction during cooling of the weld. In addition, the welding and rotation speeds will cause additional tensile stress in the weld because of the mechanical constraint of the plates by the clamps and reforming of stir zone [23].

X-ray test was performed for three cases base material, optimum case (single pass) and double pass at maximum tilting angle ($\varphi = 50^{o}$) and range of 2θ was from 30^{o} to 120^{o} to get on data and used these date to calculate residual strain from equation (**5.2**) as well as (**5.3**) to calculate residual stress [82].

From figure (5.26) the residual stress for single pass (optimum case) was 726 MPa and it higher than ultimate tensile strength of base material 280 MPa and the maximum tensile residual stress for double pass was 294 MPa and it is also higher than ultimate tensile strength for base material. Double pass led to reduce residual stress to 63.4 % due to happens homogenous distribution of residual stress in both sides (advance and return side). This reduction in value of residual stress led to increase in ultimate tensile strength, hardness and improves fatigue life for double pass (FSP). All details to calculate residual stress are presented in appendix B.

$$\varepsilon_{re} = \frac{d - d_o}{d_o} \quad \ldots\ldots\ldots\ldots\ldots\ldots\ldots\ldots (5.2)$$

$$\sigma_{re} = \frac{E}{(1+v) * (sin\varphi_1^2 - sin\varphi_2^2)} * \varepsilon_{re} \quad \ldots\ldots\ldots (5.3)$$

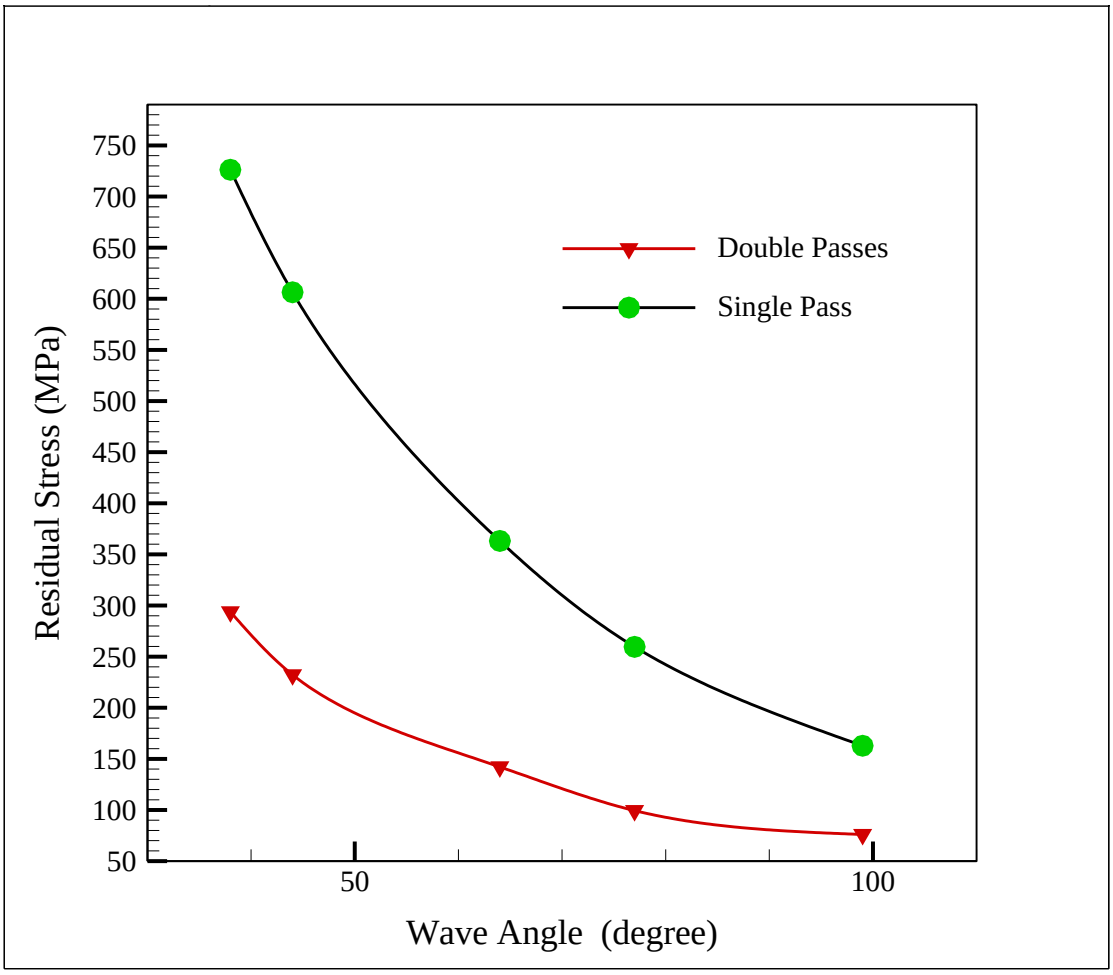

Figure (**5.17**): Residual Stresses for Single Pass and Double Pass (FSP).

5.7 Fatigue Test Results (Experimental)

The fatigue test results were performed for three cases, for the base material, the optimum case (single pass) for FSW and for double pass. The stress ratio was R = -1 and the fatigue limit considers 10^6 cycles. The load and deflection can calculate from equations (5.4, and 5.5) as shown in table (**5.9**).

$$P = \frac{\sigma_b * b * t^2}{6 * l} \quad \ldots\ldots\ldots\ldots\ldots\ldots\ldots (5.4)$$

$$\delta = \frac{4 * P * l^3}{E * b * t^3} \quad \ldots\ldots\ldots\ldots\ldots\ldots\ldots (5.5)$$

5.7.1 Case One: Fatigue Test for the Base Material

Figure (**5.18**) explained the S-N curve for base material. Nine stress levels were taken to present the S-N curve. When a decrease in the stress level the number of cycles increase and reached to infinite life (10^6) when applied stress 118 MPa.

The fracture location in base material occurs in the region very near to the supported edge because the stress in this region is very large when compared with other regions as shown in figure (**5.27**).

Table (**5.8**) the stress and deflection that are used in fatigue test for B.M

Stress (MPa)	**Force (N)**	$\delta(mm)$	**Nf (Exp.)**
250	111.11	2.173	29489
225	100	1.956	62413
190	84.444	1.652	96108
175	77.778	1.521	130398
135	60	1.173	472280
130	57.778	1.130	675513
125	55.55556	1.086	891910
118	52.444	1.026	1032649

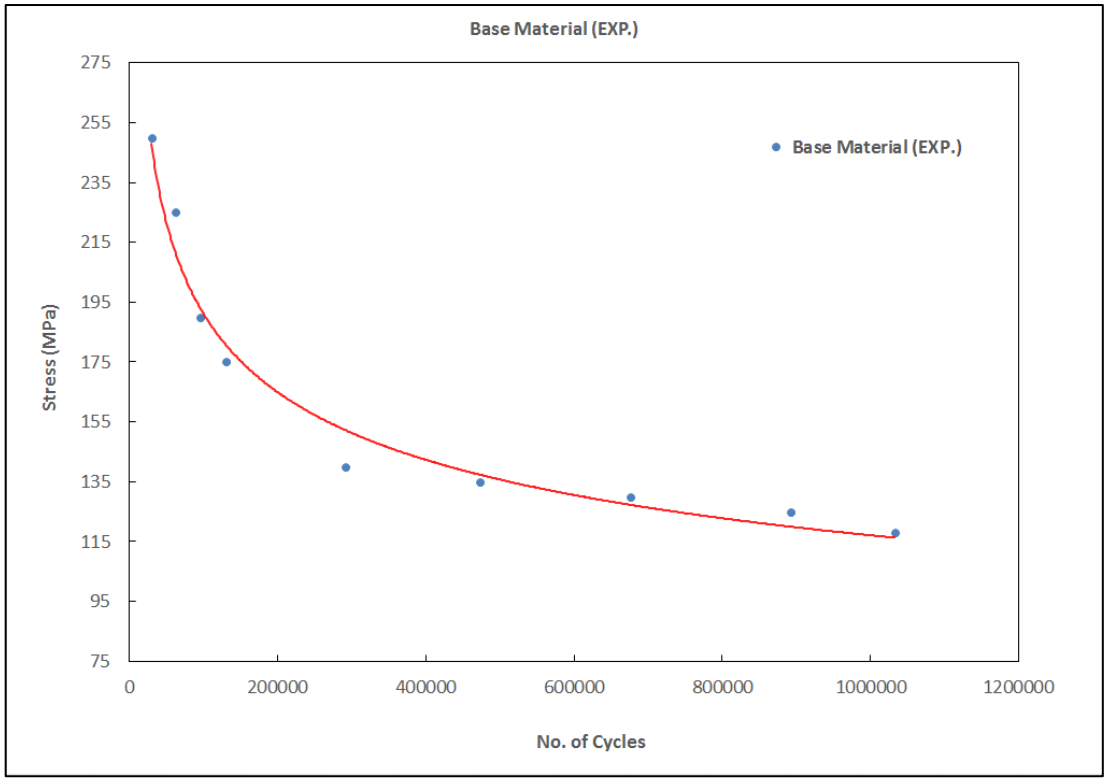

Figure (**5.18**): S-N curve for the base material.

5.7.2 Case Two: Fatigue Test for Single Pass (Optimum Case)

The higher rotation speed and lower welding speed (feed rate) are beneficial in fatigue life, and this is associated with the increased amount of heat supplied to the weld per unit length i.e. the heat generated during FS is enough to reach the metal plastic flow [78]. The figure (**5.19**) explained the S-N curve for the optimum case (single pass). Usually, the material that welded by FSW has lower ductility and strength from base material due to the softening in nuggets zone which product from the deterioration of precipitates. But the material that welded by FSW have better fatigue strength when compared with the same material that welded by traditional fusion welding [59].

Reduction in fatigue strength may be caused by the grain refinement in the nugget zone, in addition, the change in micro-hardness during the weldment. This means that there will be a significant change in the residual stresses which play an important role in the life of the weldment. In FSW all of the fracture locations occurs in the weld zone as shown in figure (**5.20**) because the region is less thickness and weaker.

Table (**5.9**) the stress and deflection that are used in fatigue test for the single pass.

Stress (MPa)	**Force (N)**	**δ(mm)**	**Nf (EXP.)**
132.45	58.86	1.34	41569
124	55	1.26	48943
115	51.133	1.17	58493
106	47	1.08	72276
90	40	0.913	218600
85.45	38	0.869	399438
81.223	36	0.826	713986

78.66	35	0.8	947026
76	34.17	0.782	1073421

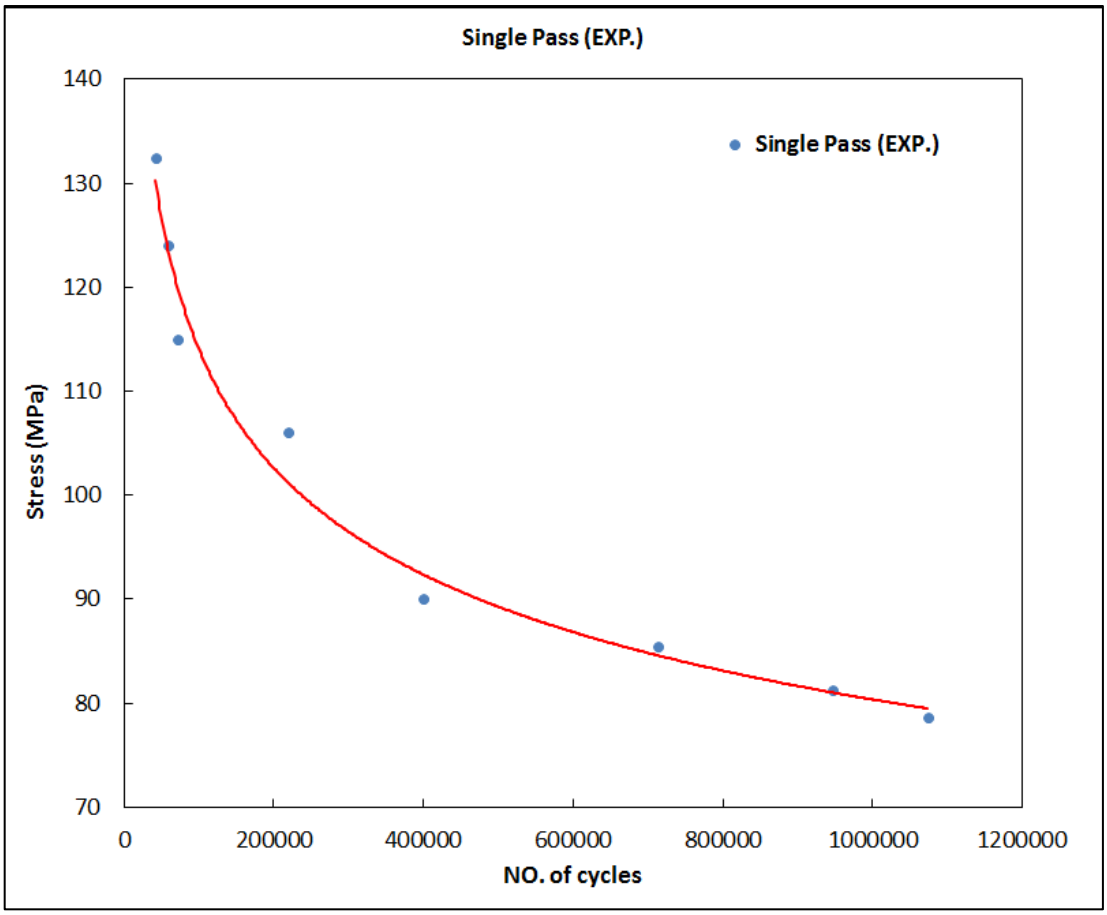

Figure (**5.19**): S-N curve for the single pass.

Figure (**5.20**): Fatigue fracture location for single pass.

5.7.3 Case Three: Fatigue Test for Double Pass (FSP)

Figure (**5.21**) explained S-N curve for double pass (FSP), at 105 MPa the number of cycles reaches to 10^6. FSP (double pass) is work on higher enhancement of fatigue life and mechanical properties due to reduction of residual stresses in weldment [36]. The position of fracture in double pass at low-level stress occurs outside weld zones but at high-level stress, the fracture occurs inside the weld zone as shown in figure (**5.22**).

Table (**5.10**) the stress and deflection that are used in fatigue test for double pass.

Stress (MPa)	**Force (N)**	$\boldsymbol{\delta(mm)}$	**Nf (EXP.)**
180	84.44	1.65	44643
163	76.889	1.50	85690
146	68.889	1.34	160140
132	62.222	1.21	281540
123	57.778	1.13	506500
113	53.333	1.04	604500
108.8	51.111	1	725735
104	48.889	0.956	1100519

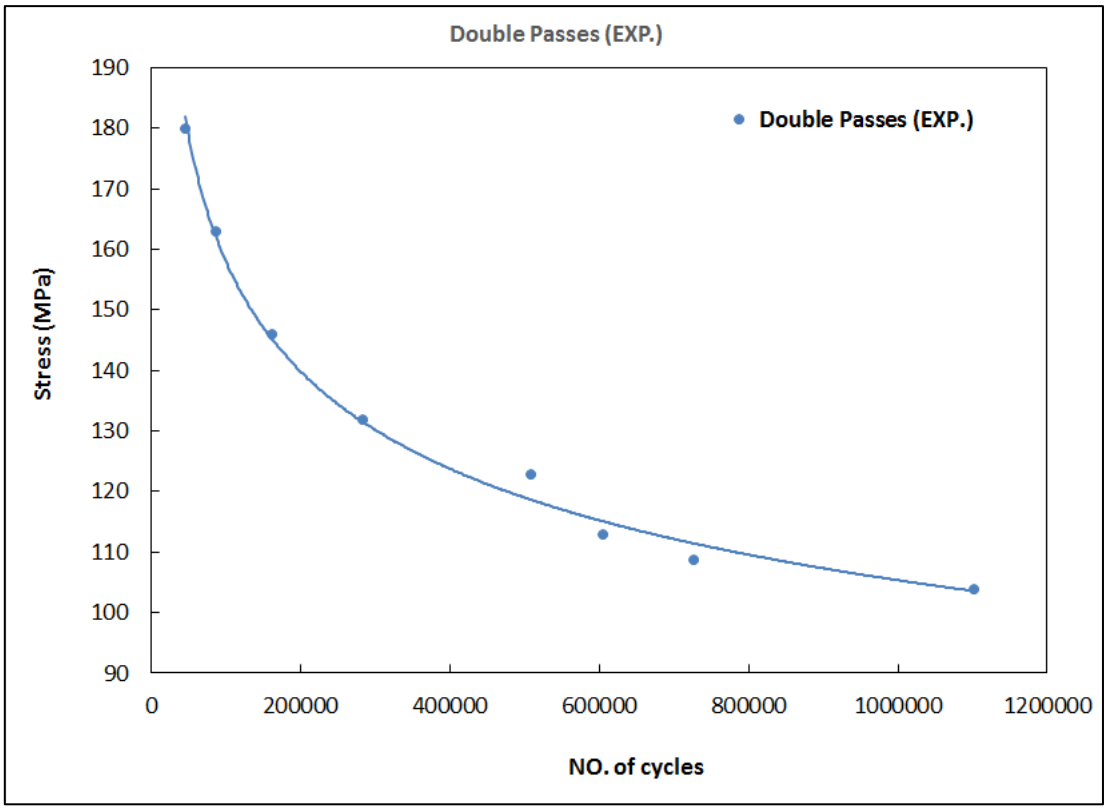

Figure (**5.21**): S-N curve for the double passes.

Figure (**5.22**) fatigue fracture location for BM and double pass (at low stress level).

5.7.4 Endurance Limit and Fatigue Curve Equations

From figure (**5.23**) the endurance limit for base material was 118.63 MPa while for double pass (FSP) was 107 MPa and for optimum case (single pass) was 82.34 MPa. The reduction in endurance limit for optimum case (single pass) FSW was 30.6 % while the reduction in double pass was 10 %, this reduction in endurance limited for optimum case (single pass) return to the lower welding speed and higher rotation speed work on increase the amount heat transfer to the material during unit length [83]. While in double pass as well as to lower welding speed and higher rotation speed, the double pass in same orientation welding speed and opposite rotation speed work on redistribution of residual stress in two sides retreating and advance sides [36].

To find fatigue curve equation and endurance limit used equations below.

$\sigma_f = AN_f^m$ ..... (5.6)

$\log \sigma_f = \log A + m \log N_f$ ..... (5.7)

σ_f The applied stress

N_f Is the fatigue life (cycle)

Table (**5.11**) Experimental fatigue Curve Equation.

Material	Curve Equation	Fatigue limit
Base Material	$\sigma_f = 2071.174N_f^{-0.207}$	118.63
Single Pass (optimum case)	$\sigma_f = 804.74N_f^{-0.165}$	82.34
Double Pass	$\sigma_f = 1119.4\ N_f^{-0.170}$	107

5.8 Numerical Fatigue Results

A. Base Material

Figures (**5.23**) to (**5.26**) explained the equivalent stress, safety of factor, total deformation and number of cycles for base material at 135MPa and other cases were calculate in the same way and it presented in tables (**5.12**) to (**5.14**) for single and double pass.

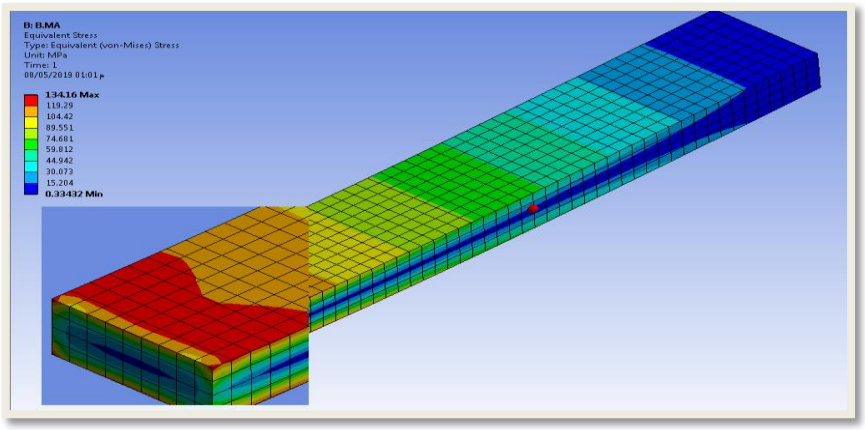

Figure **(5.23)**: Equivalent Von Misses stress for BM.

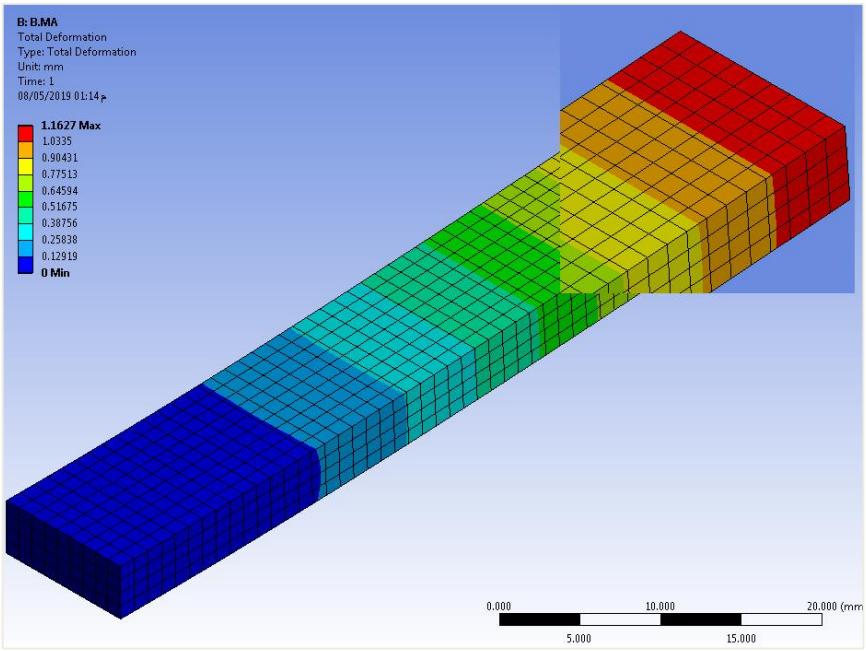

Figure (**5.24**): Total deformation for BM.

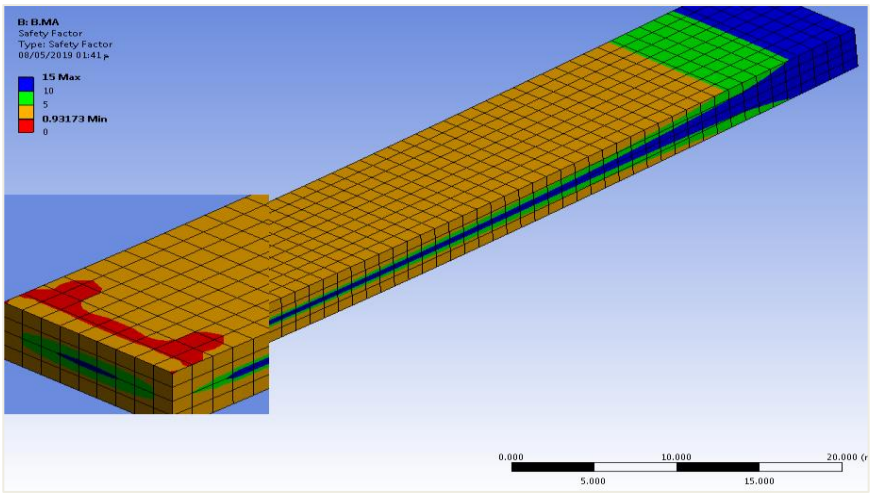

Figure **(5.25)**: Safety factor.

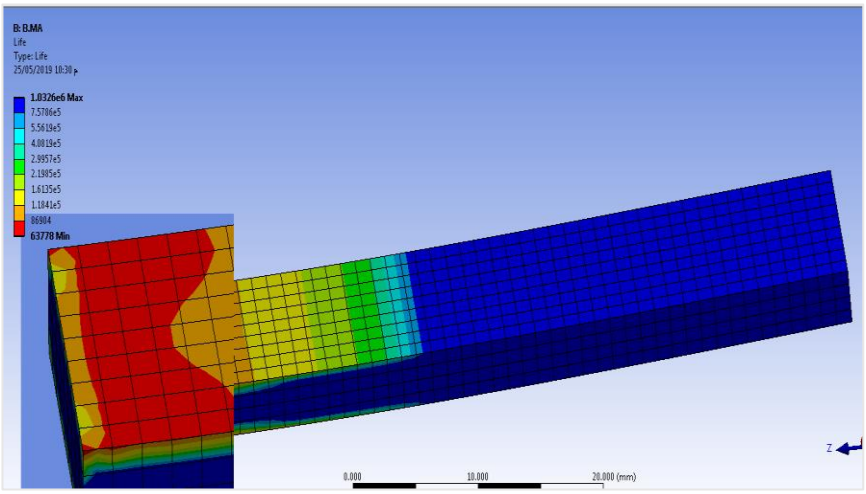

Figure **(5.26)**: Available for fatigue life for BM.

Table (**5.12**) ANSYS results for BM

Applied stress (MPa)	Total deformation (mm)	Equivalent stress (MPa)	No. of cycle to failure (Num.)	Safety factor
250	2.153	248.44	30381	0.5037
225	1.937	223.6	63778	0.559
190	1.636	188.82	98365	0.662
175	1.507	173.91	132410	0.718
135	1.162	134.16	473559	0.931
130	1.119	129.19	698420	0.96
125	1.076	124.22	892523	0.98
118	1.012	116.77	1042600	1.016

B. Single Pass (Optimum Case)

Table (**5.13**) ANSYS results for single pass

Applied stress(MPa)	Total deformation **(mm)**	Equivalent stress **(MPa)**	No. of cycle to failure (num.)	Safety factor
132.45	1.3383	131.56	40844	0.584
124	1.2519	122.93	49616	0.624
115	1.165	114.24	59973	0.6711
106	1.079	105.05	75380	0.724
90	0.95	89.405	235270	0.866

85.45	0.863	48.935	404200	0.906
81.223	0.82	80.46	714110	0.953
78.66	0.794	78.22	983500	0.984
76	0.777	76.374	1092500	1.0067

C. Double passes (FSP)

Table (**5.14**) ANSYS results for double pass

Applied stress**(MPa)**	Total deformation **(mm)**	Equivalent stress **(MPa)**	NO. of cycle to failure **(num.)**	Safety factor
180	1.64	178.98	46582	0.582
163	1.493	162.07	88370	0.639
146	1.338	145.17	163520	0.713
132	1.2088	131.25	294210	0.790
123	1.122	122.3	549050	0.85
113	1.036	112.35	628189	0.92
108.8	0.992	108.58	756120	0.961
104	0.949	103.4	1200000	1.0057

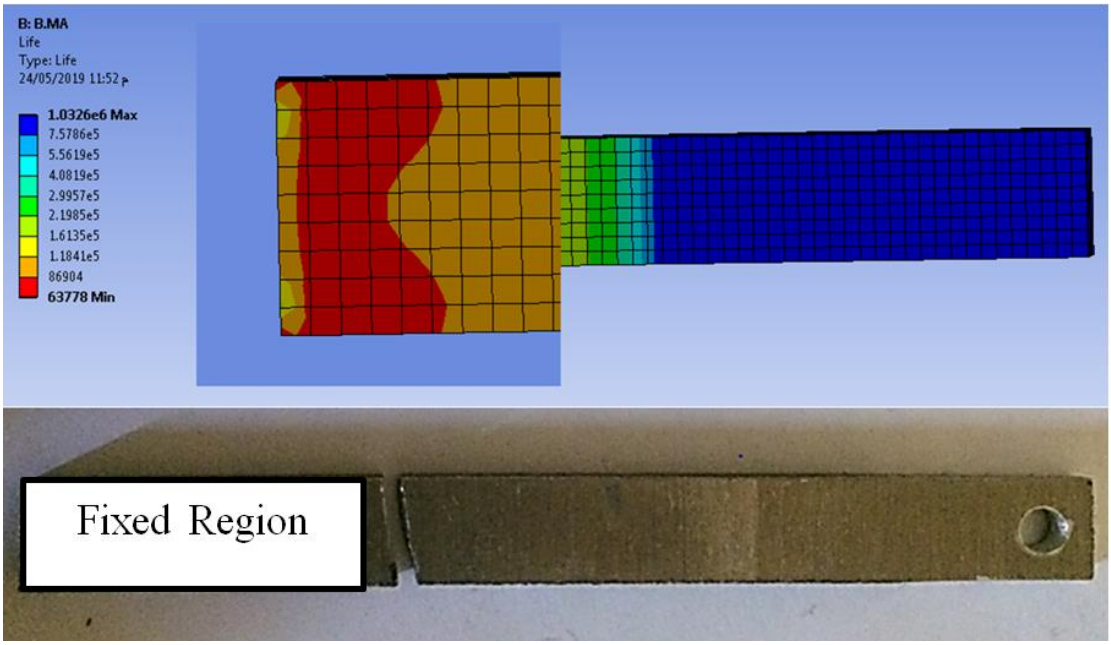

Figure (**5.27**): Fracture location for base material.

D. Endurance Limit and Fatigue Curve Equation (Numerical)

The endurance limit for base material was 119 MPa while for optimum case (single pass) was 77.5 MPa and for double pass was 107 MPa. Fatigue curve equations are explained in table (**5.16**).

Table (**5.15**) Numerical endurance limit and fatigue curve equation

Material	Curve equation (num.)	Fatigue limit
BM	$\sigma_f = 2107N^{-0.208}$	119
Single Pass	$\sigma_f = 778.55N^{-0.167}$	77.5
Double Pass	$\sigma_f = 1073.4N^{-0.167}$	106.84

5.9 Comparison Between Experimental and Numerical

The results showed that good agreement between experimental and numerical modeling, but there is a small difference in number of cycles calculated between the numerical and experimental, less than 10 % which is acceptable. The discrepancy between the numerical and experimental values was found because of the condition of the experimental work which cannot be controlled, as well as, it was not completely very precise, such as the equipment and environment. The comparisons are explained in tables (**5.16**) to (**5.18**).

Table (**5.16**) comparison between experimental and numerical for BM

Stress (MPa)	Nf (Exp.)	Nf (Exp.)	Error %
250	29489	30381	2.9
225	62413	63778	2.14
190	96108	98365	2.29
175	130398	132410	1.15
135	472280	473559	0.27
130	675513	698420	3.27
125	891910	892523	0.06
118	1032649	1042600	0.95

Table (**5.17**) comparison between experimental and numerical for single pass

Stress (MPa)	Nf (Exp.)	Nf (Num.)	Error %
132.45	40844	41569	1.74
124	48943	49616	1.35
115	58493	59973	2.46
106	72276	75380	4.11
90	218600	235270	7.08
85.45	399438	404200	1.17
81.223	713986	714110	0.017
78.66	947026	983500	3.7
76	1073421	1092500	1.74

Table (**5.18**) comparison between experimental and numerical for FSP

Stress (MPa)	Nf (Exp.)	Nf (Num.)	Error %
180	44643	46582	4.16
163	85690	88370	3.03
146	160140	163520	2.06
132	281540	294210	4.3
123	506500	549050	7.74
113	604500	628189	3.77
108.8	725735	756120	4
104	1100519	1200000	8.29